Proceedings of the International Workshop NOA'00, Grybów 2000

MAGNETO-OPTIC PERIODIC STRIP STRUCTURES

D. Ciprian* and J. Pištora

Department of Physics, Technical University Ostrava
17. listopadu 15, Ostrava, 708 33, Czech Republic

The paper deals with the optical response from periodic lamellar magnetic structure consisting of permalloy strips on Si substrate covered by Cr protection layer. The ultrathin structure is magnetized in polar geometry and the spectral dependence of magneto-optic response is computed using rigorous coupled wave analysis. The results are compared with the data obtained from magneto-optical ellipsometry experiments. Further model computation helps to understand the basic features of the Kerr rotation spectra and reveal the possible reason of deviation between the experimental data and the model computation.

PACS numbers: 42.25.Fx, 78.20.Ls, 75.70.–i

1. Introduction

The interest in the magnetic layered systems has exhibited increasing tendency in the last decade. The attention, traditionally focused on the ultrathin magnetic layers, is shifted now to the structures with lateral periodicity. New grating structures containing anisotropic materials regard generalization of methods used for isotropic grating description in order to explain experimental results. Experiments with magneto-optic diffraction were carried out, for example, with surface relief grating covered by magneto-optic material [1]. Recently, the progress of technology allowed preparation of biperiodic structures [2]. The contribution is devoted to the study of magneto-optic lamellar structure confronted with experimental results obtained from magneto-optic spectral measurement.

Theoretical description uses rigorous coupled wave approach (RCWA) sometimes called Fourier modal method (FMM). The first step is the eigenproblem formulation by direct using of the Maxwell equations. After introducing of appropriate Fourier expansion of all quantities, the normal components of the field are expressed using tangential components only. Such formulation leads to the matrix eigenvalue problem.

*corresponding author; e-mail: dalibor.ciprian@vsb.cz

Then the boundary conditions are applied, originally in the stack-matrix form. Used form of multilayer approximation in stack-matrix formulation unfortunately suffers from the so-called $\boldsymbol{T}$-matrix instability. This weak point can be removed by reformulation of boundary conditions using decreasing exponential terms only, but the size of linear equation system (simultaneous formulation of boundary conditions) rapidly increases. That is why it is better to use the method called $\boldsymbol{S}$-matrix algorithm [3]. In this case the size of the system matrix remains the same and the structure is artificially divided into elementary layers. Instead of field components, $\boldsymbol{S}$-matrices connecting together amplitudes of up and down propagating modes are calculated using a recursive algorithm. When the complex modal amplitudes are obtained, the appropriate quantities (diffraction efficiencies or ellipsometric parameters) can be calculated. In our case, the model calculations are used for qualitative explanation of experimental results obtained on double layer magnetic lamellar structure magnetized in polar geometry.

2. Rigorous coupled wave analysis

The method was developed by Moharam and Gaylord for the case of isotropic grating structures and subsequently generalized to anisotropic slanted gratings by Rokushima and Yamakita [4]. Recently, the analysis of convergence properties leading to the improved performance of the method was carried out by Li [5]. The basic idea is to expand the functions describing material parameters and electromagnetic field components into a Fourier series (Floquet modes) with one fundamental period in the system. The assumption about one common period in the periodic system represents fundamental restriction of the RCWA method.

In the further considerations, the space coordinates are normalized by vacuum wave vector $k_0 = \sqrt{\varepsilon_0 \mu_0} = 2\pi/\lambda$ ($\bar{x} = k_0 x$, $\bar{y} = k_0 y$, $\bar{z} = k_0 z$, for the rest of the paper the bar will be omitted) and all field components are harmonic functions of time $\exp(\mathrm{i}\omega t)$. As to the material parameters, all materials in the structure are expected to be non-magnetic in the sense $\mu = \mu_0$ and all the regions are completely described by their appropriate complex relative permittivity tensors $\boldsymbol{\varepsilon}$. In our case we suppose the lamellar geometry of the grating (strip structure — see Fig. 1), if the surface relief or relative permittivity profile is not lamellar, then the multilayer approximation has to be used. Each component of $\boldsymbol{\varepsilon}$ is represented by its Fourier

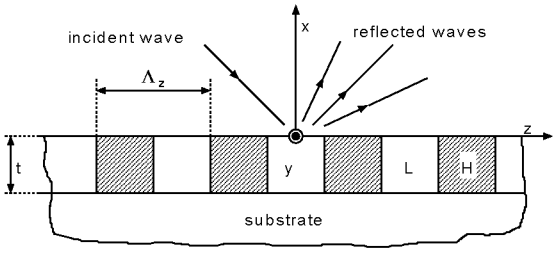

Fig. 1. Schematic drawing of lamellar grating.

expansion

$$\varepsilon_{ij}(\boldsymbol{r}) = \sum_{m=-\infty}^{+\infty} [\varepsilon_{ij}]_m \ \exp(\mathrm{i}m\boldsymbol{K}\cdot\boldsymbol{r}), \tag{1}$$

where $\boldsymbol{K} = (2\pi/\Lambda_x, 2\pi/\Lambda_y, 2\pi/\Lambda_z)$ is the grating vector, Λ_i are appropriate grating periods and $[\varepsilon_{ij}]_m$ are m-th order Fourier coefficient calculated for given material parameter profile. According to the Floquet theorem, the waves in the grating region can be expressed in the similar way

$$\sqrt{Y_0}\boldsymbol{E} = \sum_{m=-\infty}^{+\infty} \boldsymbol{e}_m(x)\exp[-\mathrm{i}(p_m x + q_m y + s_m z)], \tag{2}$$

$$\sqrt{Z_0}\boldsymbol{H} = \sum_{m=-\infty}^{+\infty} \boldsymbol{h}_m(x)\exp[-\mathrm{i}(p_m x + q_m y + s_m z)], \tag{3}$$

where $Y_0 = Z_0^{-1} = \sqrt{\varepsilon_0/\mu_0}$, $\boldsymbol{e}_m(x)$ and $\boldsymbol{h}_m(x)$ are m-th order space harmonics. The symbols $p_m = 2\pi m/\Lambda_x$, $q_m = 2\pi m/\Lambda_y$ and $s_m = s_0 + 2\pi m/\Lambda_z$, where $s_0 = \sqrt{\varepsilon_{\mathrm{sup}}}\sin\theta_i$, are related to the appropriate space harmonics, θ_i is the angle of incidence. After introducing of (2), (3) and (1) into the normalized form of Maxwell curl equations

$$\nabla\times\sqrt{Y_0}\boldsymbol{E}(\boldsymbol{r}) = -\mathrm{i}\sqrt{Z_0}\boldsymbol{H}(\boldsymbol{r}), \qquad \nabla\times\sqrt{Z_0}\boldsymbol{H}(\boldsymbol{r}) = \mathrm{i}\varepsilon_r\sqrt{Y_0}\boldsymbol{E}(\boldsymbol{r}), \tag{4}$$

a set of couple wave equations for tangential field components can be written in the compact matrix form

$$\frac{\mathrm{d}}{\mathrm{d}x}\boldsymbol{f}_t = \mathrm{i}\boldsymbol{C}\boldsymbol{f}_t, \tag{5}$$

where $\boldsymbol{C}$ is $4(2m_{\max}+1)\times 4(2m_{\max}+1)$ coupling matrix and $\boldsymbol{f}_t = (\boldsymbol{e}_y, \boldsymbol{h}_z, \boldsymbol{e}_z, \boldsymbol{h}_y)$ is the column vector consisting of space harmonics expansion coefficients of tangential field components. The derivation of the coupled wave equations is based on Beremann's work considering optics of anisotropic layered media. For details see [3] and [5]. The set of equations can be solved using diagonalization procedure for matrix $\boldsymbol{C}$. From the physical point of view, this similarity transformation means the change from the field component representation to the space harmonics amplitude representation. The transformation can be written as $\boldsymbol{f}_t = \boldsymbol{T}\boldsymbol{g}$ and the set of equation for mode amplitudes takes the following form:

$$\frac{\mathrm{d}}{\mathrm{d}x}\boldsymbol{g} = \mathrm{i}\boldsymbol{\chi}\boldsymbol{g}. \tag{6}$$

Here $\boldsymbol{g}$ is the amplitude vector and $\boldsymbol{\chi}$ is the diagonal matrix containing the χ_i eigenvalues of $\boldsymbol{C}$ on its diagonal. The matrix $\boldsymbol{T}$ is composed of appropriate eigenvectors.

The same procedure can be applied to the electromagnetic fields in uniform region of the structure (for example substrate or superstrate). In this case the material parameters do not exhibit any periodicity and the coupling matrix $\boldsymbol{C}$ takes the block diagonal form. Each 4×4 block corresponds with one diffraction order. For basic types of anisotropy, the eigenvalues and eigenvectors can be written explicitly. When the uniform region consists of isotropic material, the eigensolution

takes the form of TE and TM waves. In the uniform region, the space harmonics are uncoupled.

The main task in the grating theory is to find the complex amplitudes of space harmonics in the superstrate and substrate of the structure where they represent reflected or transmitted diffracted waves. According to the electromagnetic field theory, appropriate boundary conditions has to be fullfilled for the tangential field components on each interface. The easiest way to do that is to use the so-called $\boldsymbol{T}$-matrix method, where the field components in the superstrate and substrate are connected via the product of propagation and boundary matrices (continuity relations) of each layer in the structure. This method is used without any problem in the optics of layered media, but when it is applied to the grating theory, it exhibits devastating instability during numerical computation. The trouble arises from higher order modes, whose eigenvalues χ_i have large imaginary parts. This leads to rapidly growing exponential factors and subsequently, the total matrix of the structure is badly scaled. Such behaviour brings serious limitation in the thickness of the structure and especially surface relief gratings cannot be treated in this way. One possibility how to avoid this problem is to divide the modes in each layer in two groups — "up" and "down" propagating modes and fullfil the boundary conditions on all interfaces simultaneously (see for example [6]) using decreasing exponentials only. Unfortunately, in this case the dimension of the total matrix of the structure rapidly increases with the number of layers.

The suitable solution is to retain the concept of proper using only decreasing exponentials and to divide the structure artificially into the system of thin sublayers (the multilayer approximation is naturally included). The total matrix of the structure is computed by a recursive procedure. The method is called $\boldsymbol{S}$-matrix algorithm and its analysis was performed by Li [3].

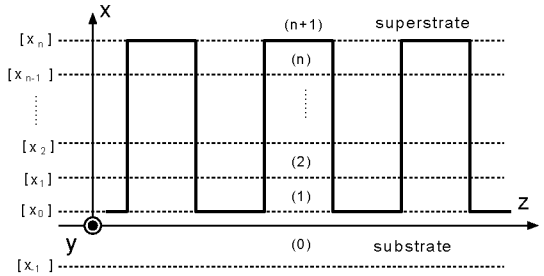

Fig. 2. Schematic drawing of layer system used for $\boldsymbol{S}$-matrix algorithm, the numbers in brackets are related to the media, square brackets denote boundaries.

Here, we briefly review basic ideas of the method. The structure is artificially divided into n elementary sublayers (see Fig. 2), the waves are distinguished according to their transverse direction of propagation. The appropriate wave amplitudes constitute two vectors: $\boldsymbol{u}$ contains the amplitudes of waves propagating in the $+x$ direction ("up" modes), whereas $\boldsymbol{d}$ is related to $-x$ direction ("down" modes). In order to use decreasing exponential terms only, one seeks the matrix $\boldsymbol{S}$

connecting the wave amplitudes in the following way:

$$\begin{bmatrix} \boldsymbol{u}^{(n+1)} \\ \boldsymbol{d}^{(0)} \end{bmatrix} = \boldsymbol{S}^{(n)} \begin{bmatrix} \boldsymbol{u}^{(0)} \\ \boldsymbol{d}^{(n+1)} \end{bmatrix}, \tag{7}$$

where index (0) denotes the substrate and $(n+1)$ superstrate. This matrix can be computed using interface matrices $\boldsymbol{s}$ connecting the wave amplitudes in two adjacent layers (j) and $(j+1)$ in the same way as (7)

$$\begin{bmatrix} \boldsymbol{u}^{(j+1)}[x_j+0] \\ \boldsymbol{d}^{(j)}[x_j-0] \end{bmatrix} = \boldsymbol{s}^{(j)} \begin{bmatrix} \boldsymbol{u}^{(j)}[x_j-0] \\ \boldsymbol{d}^{(j+1)}[x_j+0] \end{bmatrix}, \tag{8}$$

where the symbols +0 and –0 denote the direction in which we are approaching the j-th boundary. The interface matrix $\boldsymbol{s}^{(j)}$ can be calculated either from boundary matrix $t^{(j)} = [\boldsymbol{T}^{(j+1)}]^{-1}\boldsymbol{T}^{(j)}$, or directly from $\boldsymbol{T}^{(j+1)}$ and $\boldsymbol{T}^{(j)}$ elements (for details see [3]). The propagation across the layer in transverse direction is introduced using the matrix $\tilde{\boldsymbol{s}}^{(j)}$ which uses only decreasing exponential propagation factors (d_j are layer thicknesses)

$$\tilde{\boldsymbol{s}}^{(j)} = \begin{bmatrix} \mathbf{1} & 0 \\ 0 & \exp[-\mathrm{i}\boldsymbol{\chi}^{(j)+}d_j] \end{bmatrix} \boldsymbol{s}^{(j)} \begin{bmatrix} \exp[-\mathrm{i}\boldsymbol{\chi}^{(j)-}d_j] & 0 \\ 0 & \mathbf{1} \end{bmatrix}. \tag{9}$$

During the process of computation, the matrix $\boldsymbol{S}^{(j)}$, which connects the field amplitudes on both sides of stack of j layers is computed using $\boldsymbol{S}^{(j-1)}$ and $\tilde{s}^{(j)}$. For this purpose, the set of recursive formulae can be written in the following form:

$$\begin{aligned}
S_{11}^{(j)} &= \tilde{s}_{11}^{(j)}[1 - S_{12}^{(j-1)}\tilde{s}_{21}^{(j)}]^{-1}S_{11}^{(j-1)}, \\
S_{12}^{(j)} &= \tilde{s}_{12}^{(j)} + \tilde{s}_{11}^{(j)}S_{12}^{(j-1)}[1 - \tilde{s}_{21}^{(j)}S_{12}^{(j-1)}]^{-1}\tilde{s}_{22}^{(j)}, \\
S_{21}^{(j)} &= S_{12}^{(j-1)} + S_{22}^{(j-1)}\tilde{s}_{22}^{(j)}[1 - S_{12}^{(j-1)}\tilde{s}_{21}^{(j)}]^{-1}S_{11}^{(j-1)}, \\
S_{22}^{(j)} &= S_{11}^{(j-1)}[1 - \tilde{s}_{21}^{(j)}S_{12}^{(j-1)}]^{-1}\tilde{s}_{11}^{(j)},
\end{aligned} \tag{10}$$

where the recursion can be started by setting $\boldsymbol{S}^{(0)} = \boldsymbol{s}^{(0)}$ and the symbols S_{ij} and $\tilde{s}_{ij}$ are related to appropriate matrix blocks. The amplitudes of reflected and transmitted waves can be easily obtained from total matrix $\boldsymbol{S}^{(n)}$ as

$$\boldsymbol{u}^{(n+1)} = S_{12}^{(n)}\boldsymbol{d}^{(n+1)}, \qquad \boldsymbol{d}^{(0)} = S_{22}^{(n)}\boldsymbol{d}^{(n+1)}. \tag{11}$$

When the complex wave amplitudes are obtained, then diffraction efficiencies and ellipsometric quantities can be calculated. The diffraction efficiencies of n-th order are defined as the ratio of the power carried by the reflected or transmitted wave of the appropriate order to the power carried by the zero-order incident wave and they are done by the ratio of normal components of the Poynting vector. For example, appropriate expressions for the reflection of TE wave (s-polarization) are

$$\eta_{rn}^{ss} = \frac{\mathrm{Re}[\chi_n^{(\mathrm{sup})+}]}{\mathrm{Re}[\chi_0^{(\mathrm{sup})-}]}||g_{(\mathrm{sup})n}^{\mathrm{TE}+}||^2, \qquad \eta_{rn}^{sp} = \frac{\mathrm{Re}[\chi_n^{(\mathrm{sup})+}]}{\mathrm{Re}[\chi_0^{(\mathrm{sup})-}]}||g_{(\mathrm{sup})n}^{\mathrm{TM}+}||^2, \tag{12}$$

for transmission diffraction efficiencies hold similar formulae

$$\eta_{tn}^{ss} = \frac{\mathrm{Re}[\chi_n^{(\mathrm{sub})-}]}{\mathrm{Re}[\chi_0^{(\mathrm{sup})-}]} ||g_{(\mathrm{sub})n}^{\mathrm{TE}-}||^2, \qquad \eta_{tn}^{sp} = \frac{\mathrm{Re}[\chi_n^{(\mathrm{sub})-}]}{\mathrm{Re}[\chi_0^{(\mathrm{sup})-}]} ||g_{(\mathrm{sub})n}^{\mathrm{TM}-}||^2. \tag{13}$$

In both cases we assumed that the amplitude of the incident wave was normalized to unity. Usually, the magneto-optic effects connected with the polarization conversion are very small and it is hard to detect them using conversion diffraction efficiencies. Then it is better to use ellipsometric methods. In this case, instead of diffraction efficiencies, the quantities related to polarization state are used in the form of complex reflection and transmission coefficients for every n-th diffraction order

$$r_n^{ss} = \frac{g_{(\mathrm{sup})n}^{\mathrm{TE}+}}{g_{(\mathrm{sup})0}^{\mathrm{TE}-}}, \quad r_n^{sp} = \frac{g_{(\mathrm{sup})n}^{\mathrm{TM}+}}{g_{(\mathrm{sup})0}^{\mathrm{TE}-}}, \quad t_n^{ss} = \frac{g_{(\mathrm{sub})n}^{\mathrm{TE}-}}{g_{(\mathrm{sup})0}^{\mathrm{TE}-}}, \quad t_n^{sp} = \frac{g_{(\mathrm{sub})n}^{\mathrm{TM}-}}{g_{(\mathrm{sup})0}^{\mathrm{TE}-}}. \tag{14}$$

Using those complex coefficients, polarization state quantities are introduced in the form of complex Kerr rotation (for reflected light) and complex Faraday rotation (for transmitted light), where the real part represents the polarization plane rotation and the imaginary part the ellipticity of the wave (the example of s and p complex Kerr effect)

$$\phi_{Ks,n} = \theta_{Ks,n} + \mathrm{i}\varepsilon_{Ks,n} = \frac{r_n^{sp}}{r_n^{ss}}, \quad \phi_{Kp,n} = \theta_{Kp,n} + \mathrm{i}\varepsilon_{Kp,n} = -\frac{r_n^{ps}}{r_n^{pp}}. \tag{15}$$

The above stated formulae hold in the case, when the magneto-optic effects are small, ie. $\phi_{K,n} \approx 0$ and $\varepsilon_{K,n} \approx 0$.

3. Experimental and calculated data

The RCWA method, briefly described in the previous parts was used for model calculation considering magnetic strip structure. The structure consists of permalloy strips covered by Cr cover layer in order to protect the strips against atmospheric oxidation (see Fig. 3). The composition of permalloy was $Fe_{20}Ni_{80}$, and the structure was prepared by rf sputtering on Si substrate. The strip period Λ_z varied from 910 to 970 nm and the strip width w changes from 630 to 700 nm. The

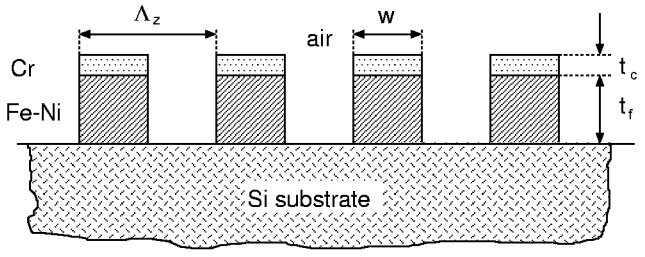

Fig. 3. Schematic drawing of double-layer magnetic periodic strip structure.

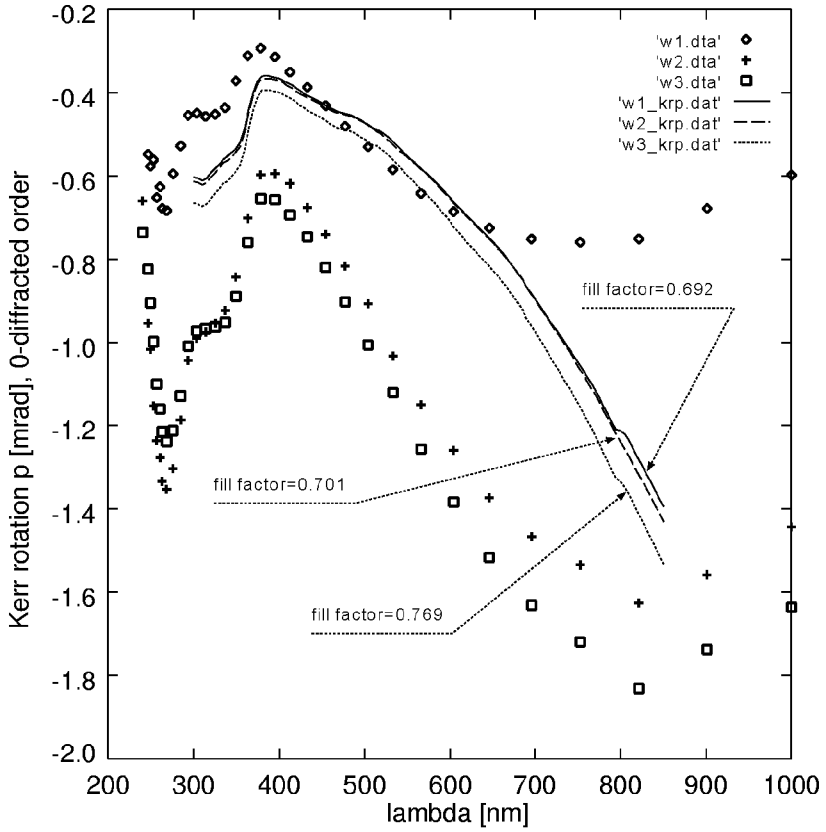

Fig. 4. Kerr rotation p spectra, comparison of experimental (points) and calculated data (lines).

thickness of the permalloy layer t_c was 10 nm and the Cr cover layer thickness was 2 nm. The structure was magnetized in polar geometry (the magnetization is perpendicular to the surface of the sample) and it was studied using magneto-optical ellipsometry. During the measurement of the Kerr effect, the spectral dependence of p Kerr rotation was obtained in the spectral region 240 nm to 1 μm for the

TABLE

Geometric parameters of samples.

Sample	Film thickness [nm]	Cover thickness [nm]	Period [nm]	Strip width [nm]	Fill factor
w1	10	2	910	630	0.692
w2	10	2	970	680	0.701
w3	10	2	910	700	0.769

samples denoted here as w1, w2, and w3 (see Fig. 4). The geometric parameters of the samples are summarized in Table. The experiments were carried out under the condition that the samples were magnetized to their saturation state. Because of the geometry of the experimental setup, the measurements were performed for $\theta_i = 7°$ angle of incidence and only the data for specular reflection (zero diffraction order) were available. The comparison of measured and computed Kerr data are depicted in Fig. 4 for all three samples. Although the model computation describes qualitatively the basic features of the spectra in visible region, there is a quantitative disagreement in the near IR region. In the following sections we make an attempt to explain the behaviour of the optical response of the structure using further model computation carried out for the samples w1 and w2.

4. Discussion

All the computed results were obtained with maximum mode order in the approximation equal to 40. In this part we tried to show the influence of the grating geometry on the Kerr rotation in the 300–850 nm spectral region. In near UV and IR the spectral dependence of permalloy material constants were not available.

The basic character of the spectra manifested by the peak near 400 nm is done by the spectral dependence of materials parameters of the substrate, where they undergo dramatic changes. This behaviour is reproduced in quantities describing the structure response — the example (w1 sample) can be seen in Fig. 5, where total absorption in the structure is depicted for s and p incident polarization. The losses are defined as the difference between 1 and the sum of all reflection and transmission diffraction efficiencies. The same features exhibit the η_{r0}^{ss} and η_{r0}^{pp} efficiencies (see Fig. 6).

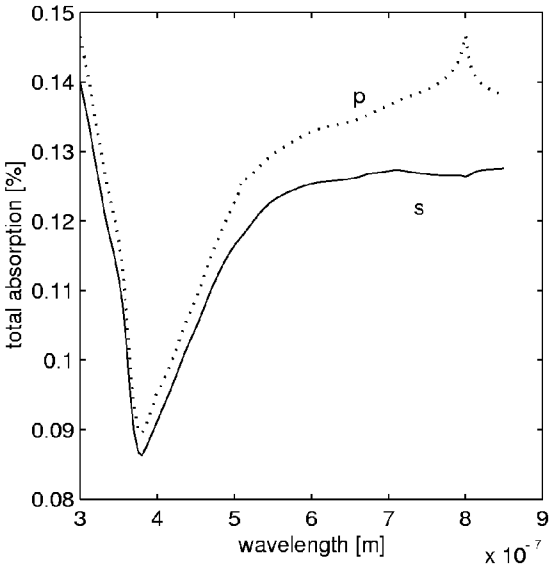

Fig. 5. Total losses.

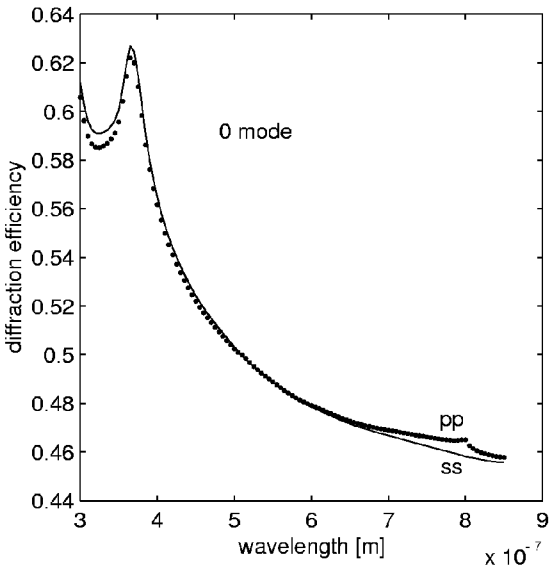

Fig. 6. η_{r0}^{ss} and η_{r0}^{pp}.

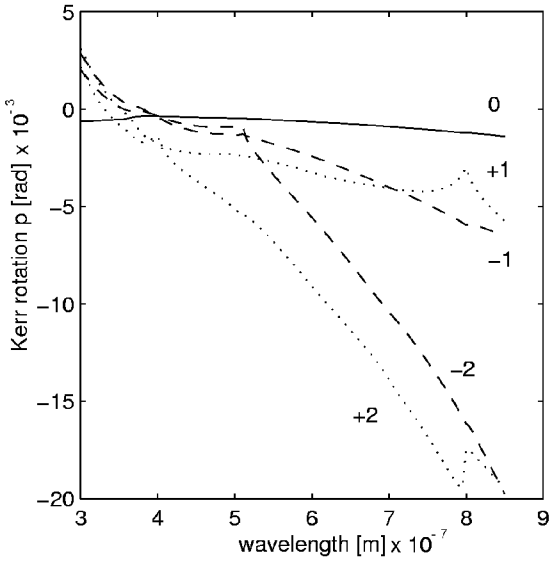

Fig. 7. Kerr rotation p.

Because the change of polarization state represented in experiment by the Kerr rotation (see Fig. 7) is connected with the power conversion, we calculated appropriate η_{rn}^{ps} diffraction efficiency for $n = -1, 0, +1$. As to Fig. 8, one has to take in mind that for higher diffraction orders the waves are purely evanescent for $\lambda > \lambda_{\mathrm{R}}$, where λ_{R} is the appropriate Rayleigh wavelength. The position of the Rayleigh wavelength is clearly seen in Fig. 9 and Fig. 10, where the η_{rn}^{ss} and η_{rn}^{pp}

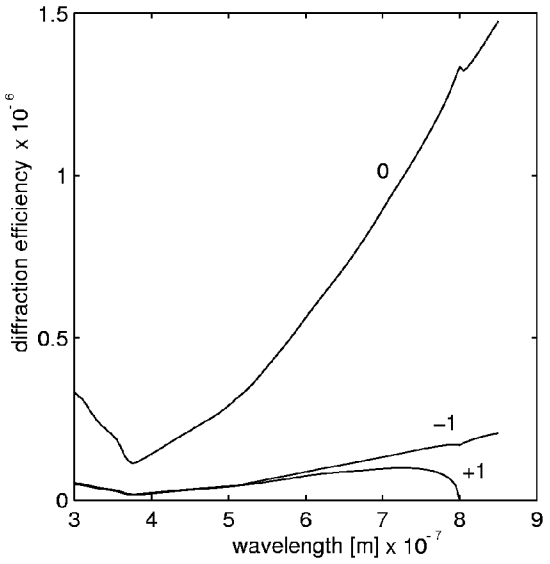

Fig. 8. Diffraction efficiency η_{rn}^{ps}.

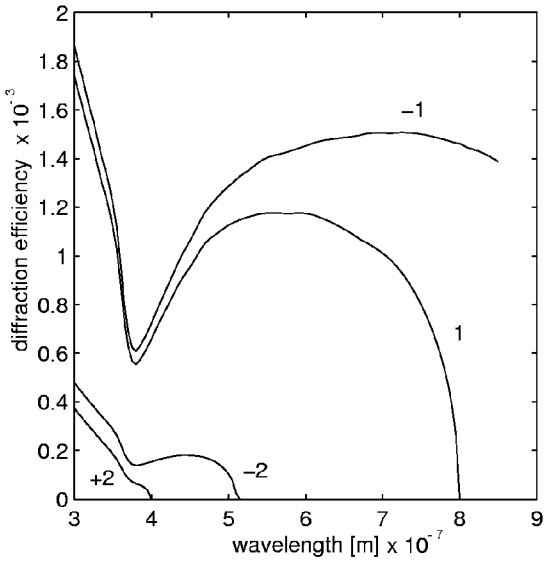

Fig. 9. Diffraction efficiency η_{rn}^{ss}.

are computed for higher diffraction orders ($n = -2 \ldots +2$). In all figures, it can be clearly seen that p polarized waves exhibit stronger intermodal coupling than the s polarized waves and the effect is more pronounced for positive diffraction orders. The behaviour near the Rayleigh resonances has to be naturally manifested in the jumps of the Kerr rotation (see Fig. 7), although the effect is not so pronounced as in the case of diffraction efficiencies.

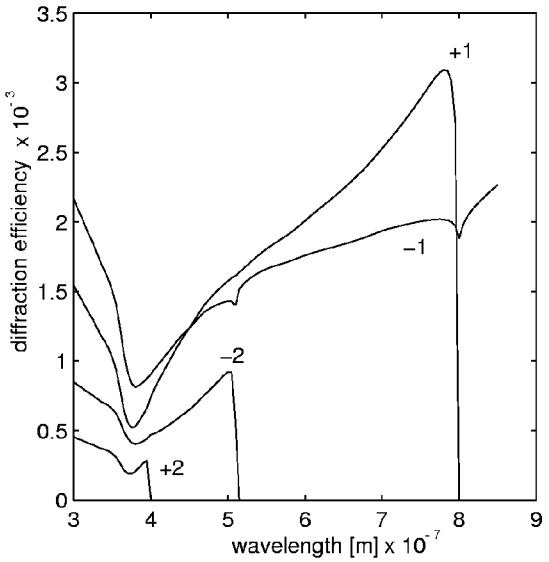

Fig. 10. Diffraction efficiency η_{rn}^{pp}.

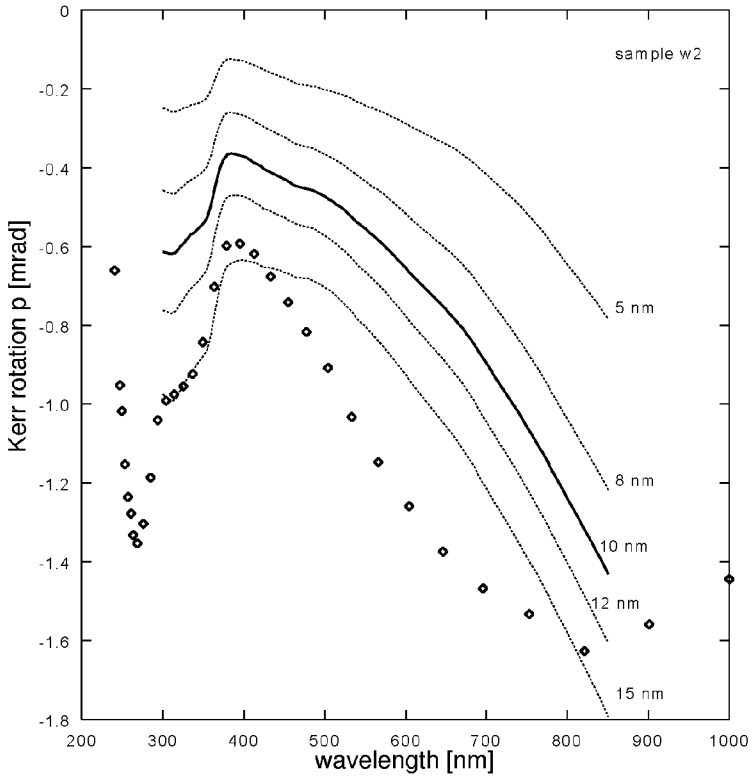

Fig. 11. Film thickness influence.

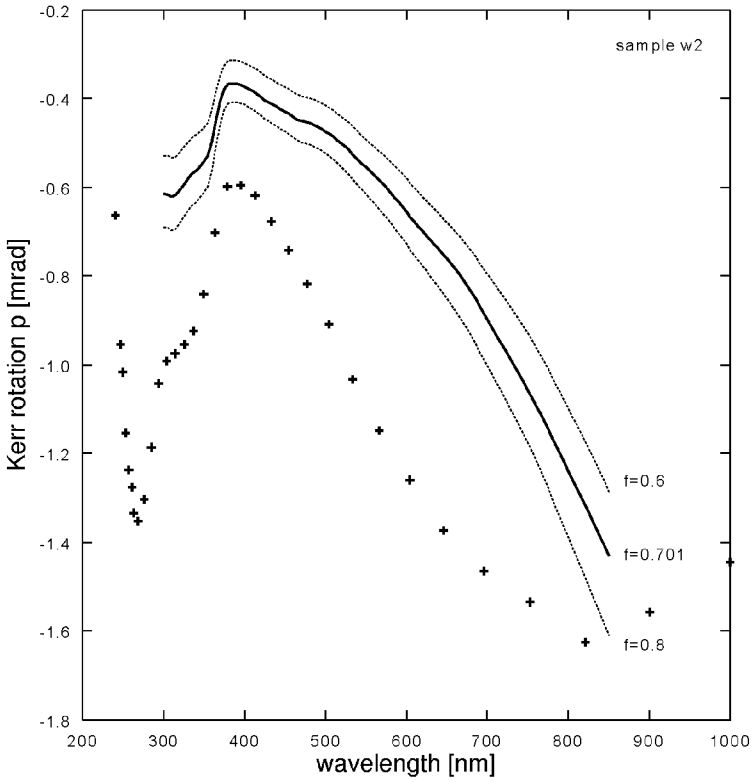

Fig. 12. Fill factor influence.

We have oriented our attention to the shape of the spectra so far, now we try to explain the reason why in the case of the w2 and w3 sample the calculated curves are shifted with respect to the experimental points. The model computation in this part of text are related to the w2 sample.

At first, the influence of the layer thickness t_f was examined. For that purpose, the Kerr rotation p spectra were computed for 5, 8, 10, 12, and 15 nm film thicknesses. The results are depicted in Fig. 11. When the thickness increases, the magneto-optic effect became stronger and the curves are shifted to the higher values of the Kerr rotation almost without any change of their shapes. It seems that the structure is too thin to support transversal resonances which could influence the shape of the spectra. The change of fill factor (defined as the ratio of the strip width to the period) has the similar effect — see Fig. 12.

The last geometric parameter, which could influence the spectra, was the cover layer thickness t_c. In order to highlight this influence, we computed the spectra for five different values of t_c. Increasing thickness of cover layer induced the decrease in the Kerr rotation magnitude, the shape of the spectra changes only slightly as can be seen in Fig. 13. It is natural to consider that the cover layer acts as the shield against the incident waves because of its absorption — the highest values of magneto-optic effect are related to the bare permalloy strips.

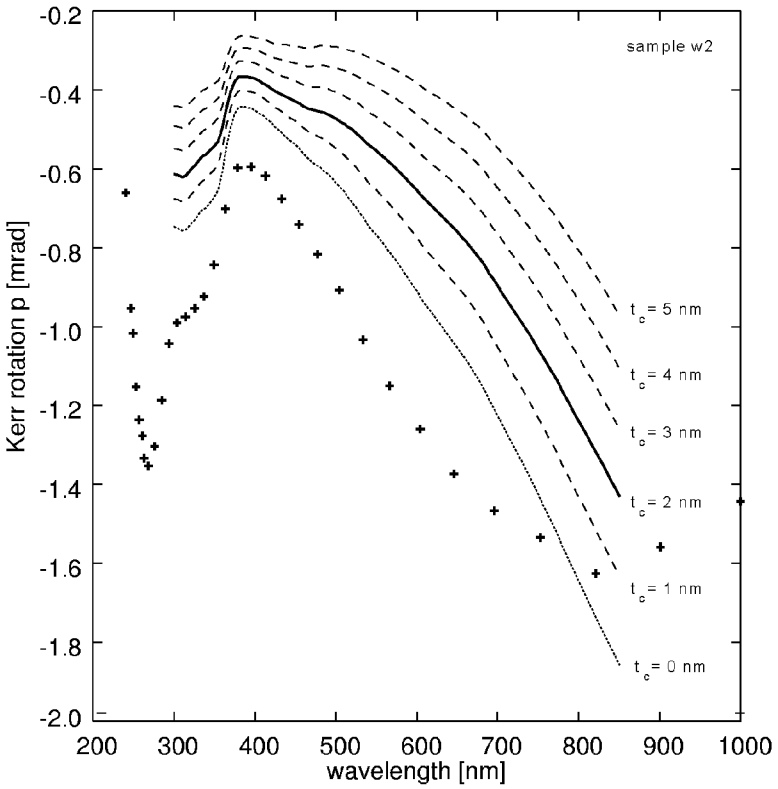

Fig. 13. Cover layer thickness influence.

5. Conclusion

The magnetic periodic strip layer structure was studied using RCWA method and the computed results were compared with data obtained from magneto-optical ellipsometry. It was shown that the quantitative disagreement between computed and experimental data in the visible region can be caused by lower accuracy of geometric parameter values (film thickness, cover thickness, and fill factor) used as input data to the model. Using the variation of those parameters, the compute curves could be successfully fitted to the experimental data. The qualitative disagreement in the shape of the Kerr rotation spectra pronounced in near IR has its origin probably in poor spectral characterization of material parameters of the structure. The most probable source of deviation can be the data of permalloy.

Acknowledgments

The authors want to express their thanks to Prof. B. Hillebrands from Kaiserslautern University, Germany, whose group prepared the samples and to

Prof. Š. Višňovský from Institute of Physics, Charles University, Czech Republic, who provided us the experimental data. This work has been partially supported by the Ministry of Education of Czech Republic under research project CEZ:J17/98:272400019 and under the projects KONTAKT No. 174 (2000) and No. 175 (2000).

References

[1] S. Gadetsky, I. Syrgabaev, J.K. Erwin, M. Mansuripur, T. Suzuki, M. Ruane, *J. Opt. Soc. Am. A* **13,** 314 (1996).

[2] N. Bardou, B. Bartenlian, J. Ferre, *J. Magn. Magn. Mater.* **148,** 293 (1996).

[3] Lifeng Li, *J. Opt. Soc. Am. A* **13,** 1024 (1996).

[4] K. Rokushima, J. Yamakita, *J. Opt. Soc. Am.* **73,** 901 (1983).

[5] Lifeng Li, *J. Mod. Opt.* **45,** 1313 (1998).

[6] K. Rokushima, J. Yamakita, S. Mori, K. Tominaga, *IEEE Trans. Microwave Theory Tech.* **35,** 937 (1987).